standards

MDPI

Article

Detecting the Corrosion of a Steel Rebar Using the Eddy Current Testing Method

Dongfeng He

National Institute for Materials Science, 1-2-1 Sengen, Tsukuba 305-0047, Japan; he.dongfeng@nims.go.jp; Tel.: +81-29-859-2533

Abstract: The corrosion of the steel reinforcing bar (rebar) reduces the strength capacity of concrete structures. Corrosion detection at the early stage of steel rebar implementation is important for the maintenance of concrete structures. Using the eddy current testing method, we developed a portable system to evaluate the corrosion of steel rebars. An AC current was sent to the excitation coil to produce an AC magnetic field and an eddy current was induced in the steel rebar. A detection coil was used to detect the signal produced by the eddy current. A lock-in amplifier was used to obtain the same phase signal and a 90-degree phase difference signal and an X-Y graph was plotted. From the slope of the X-Y graph, the corrosion of the steel rebar or steel wire can be evaluated. We examined the effects of excitation frequency, coil type, and coil size on the experimental results to optimize the system. The signal-to-noise ratio and the detection depth were improved with a specially designed probe.

Keywords: corrosion; steel rebar; eddy current testing

1. Introduction

The major cause of failure in concrete construction is the corrosion of the steel rebar. The corrosion of the steel rebar in concrete structures not only reduces the strength of the concrete structures but also causes cracking of the concrete due to the increasing volume of the corrosion products [1,2]. Water, moisture, and chloride ions can reach the rebar through the cracks, which accelerates the corrosion of the steel rebar [3]. The periodic inspection of the steel rebar in concrete is necessary and important. Knowing the conditions of the steel rebar, such as the location, the diameter, and the corrosion of the steel rebar, is important for the safety evaluation of concrete structures.

Potential measurements and resistivity measurement are used to monitor the corrosion speed of steel rebars [4–7]. Electrodes are needed and the degree of corrosion cannot be detected by this method. Ultrasonic guided waves are used to monitor the corrosion of steel rebars [8], but coupling gel is needed and the stone and void increase the measurement noise. The magnetic flux leakage (DC magnetic field excitation) method [9–11], the eddy current testing (AC magnetic field excitation) method [12–17], the microwave radar detection method [18–20], eddy-current-induced thermography technology [21,22], and the X-ray method [23,24] are non-contact methods to evaluate the location, the break, or the corrosion of the steel rebar in concrete. The magnetic flux leakage (MFL) method is mainly used to detect breaks in the prestressing steel of pre-tensioned and post-tensioned concrete structures. The microwave radar detection method can be used to detect the position and the covering depth of the steel rebar; however, the water or moisture in the concrete structures may influence the detection accuracy and it is difficult to detect the second layer of the steel rebar for concrete with a steel rebar grid. Due to the heat insulation effect of the cement, the detection depth of thermography technology is limited to about 2 cm and the devices are too heavy to be used in field experiments. The X-ray method can quantitatively evaluate the corrosion of steel rebars, but it has the disadvantages of being a potential health hazard, being a time-consuming process, and having limited portability.

check for updates

Citation: He, D. Detecting the Corrosion of a Steel Rebar Using the Eddy Current Testing Method. *Standards* **2024**, *4*, 286–299. https://doi.org/10.3390/standards4040014

Academic Editor: Humberto Varum

Received: 31 October 2024
Revised: 12 December 2024
Accepted: 18 December 2024
Published: 19 December 2024

Copyright: © 2024 by the author. Licensee MDPI, Basel, Switzerland. This article is an open access article distributed under the terms and conditions of the Creative Commons Attribution (CC BY) license (https://creativecommons.org/licenses/by/4.0/).

Compared with other methods, the low-frequency electromagnetic induction method or eddy current testing method has the advantages of low cost and easy operation. It can be used to detect the covering depth, the diameter, and the corrosion of the steel rebar. For the low-frequency electromagnetic method, the moisture of concrete also has less influence on the detection results. We developed electromagnetic evaluation methods to detect the corrosion of steel rebar [25]. Using a similar system, we also evaluated the corrosion of the steel wires used in suspension bridge cables [26]. To optimize the system, in this paper, we examine the effects of excitation frequency, coil type, and coil size on the experimental results. The signal-to-noise ratio and the detection depth are improved with a specially designed probe.

2. Materials and Methods

In different environments, a rebar generates different corrosion products. These corrosion products have different colors, electrical conductivities, and permeabilities. Table 1 lists several common corrosion products of steel rebars. The red rust is mainly composed of $Fe_2O_3 \cdot H_2O$. It is the result of heavy exposure to air and moisture, often combined with a contaminant (salt). The yellow rust is mainly composed of $FeO(OH)H_2O$. It is a result of very high moisture content. It is frequently found in settings where puddled/standing water has most likely been present. The brown rust is mainly composed of Fe_2O_3. It is a result of a high-oxygen and low-moisture environment. Brown rust is sometimes localized rust that appears as non-uniform spots or only in certain areas rather than over the whole surface. It can be the result of a contaminate on the metal's surface, often originating from the manufacturing process. The black rust is mainly composed of Fe_3O_4. It is a result of oxidation in a low-oxygen environment. Black rust almost has the appearance of a black stain. Most likely, the areas exhibiting the black rust had something covering them, which prevented oxygen from reaching the surface. This type of rust is a more stable rust layer that does not propagate as rapidly as other rust forms.

Table 1. Permeabilities and conductivities of steel rebar and its corrosion products.

Corrosion Products	Electrical Conductivity (S/m)	Relative Permeability
$Fe_2O_3 \cdot H_2O$ (red rust)	10^{-6}~10^{-4}	1.01~1.1
$FeO(OH)H_2O$ (yellow rust)	10^{-6}~10^{-4}	1.01~1.1
Fe_2O_3 (brown rust)	10^{-9}~10^{-7}	1.05~1.2
Fe_3O_4 (black rust)	10^{-2}~10^{-1}	Hundreds
Steel rebar	10^{6}~10^{7}	Hundreds

$Fe_2O_3 \cdot H_2O$ and $FeO(OH)H_2O$ typically have low electrical conductivity, ranging from about 10^{-6} S/m to 10^{-4} S/m. Both exhibit weak ferromagnetism, and their relative permeabilities are about 1.01~1.1, depending on the specific material properties and conditions. Fe_2O_3 is generally a poor conductor of electricity, with electrical conductivity typically in the range of 10^{-9} S/m to 10^{-7} S/m. Fe_2O_3 exhibits weak ferromagnetic properties. Its relative permeability is generally in the range of 1.05 to 1.2, depending on the specific conditions and crystal structure. Fe_3O_4 is known to be a good conductor of electricity compared to other iron oxides. Its electrical conductivity typically ranges from about 10^{-2} S/m to 10^{-1} S/m. Fe_3O_4 exhibits significant ferromagnetic properties. Its relative permeability is generally higher than that of many other corrosion products of steel rebar, often in the range of ten to several hundred [27]. For the steel rebar without corrosion, the electrical conductivity ranges from 10^6 S/m to 10^7 S/m and relative permeability ranges from 100 to 500. The corrosion products have different electrical and magnetic conductivities, so the corrosion of steel bars can be detected by the eddy current method.

Figure 1 shows the steel rebar used in the experiments. (a) is a 16 mm diameter deformed steel bar without corrosion. (b) is a 16 mm diameter steel rebar with corrosion, which is a naturally corroded sample from a concrete structure. There is black rust that is about 0.1 mm thick on the surface of the steel rebar.



Figure 1. (**a**) Steel rebar without corrosion. (**b**) Corroded steel rebar with black rust on the surface.

Figure 2 shows the block diagram of the rebar corrosion evaluation system using the eddy current testing method. An alternating current flows in the excitation coil and an AC magnetic field is produced. Then, an eddy current is induced in the steel rebar. The detection coil is used to measure the magnetic field produced by the eddy current of the steel rebar. The lock-in amplifier is used to obtain the X and Y signals, where the X signal is the same phase signal with the excitation magnetic field, and the Y signal is the 90-degree phase difference signal with the excitation magnetic field. The X-Y graph is plotted using the X signal and the Y signal. From the X-Y graph's slope, the steel rebar's corrosion can be detected.

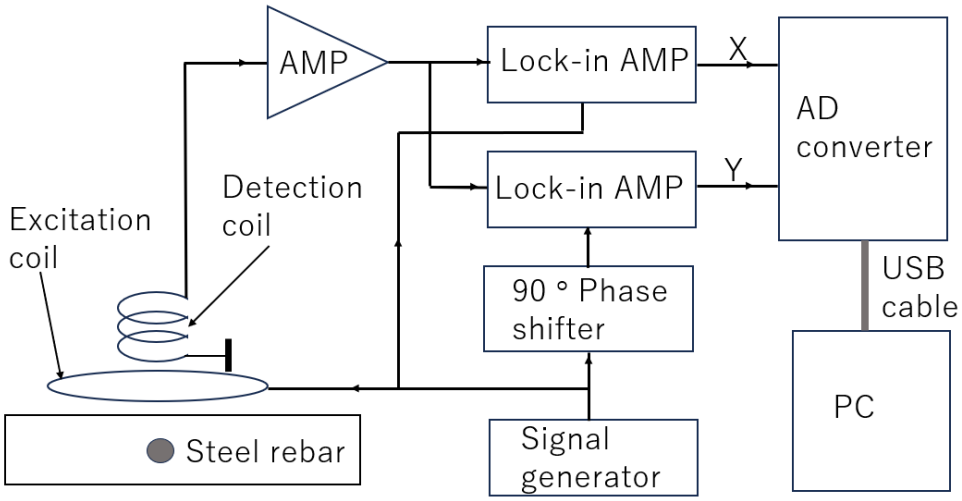


Figure 2. Block diagram of steel rebar corrosion evaluation system using the eddy current testing method.

The excitation coil and the detection coil were wound using copper wires. The amplifier was made using an AD797 (Analog Devices, Inc., Cambridge, MA, USA) op amp. The AD797 is a low-distortion and low-noise operation amplifier. The op amp with a low harmonic distortion of −120 dB is perfect for the wide dynamic range necessary for precision applications. The voltage noise is about 1 nV/$\sqrt{\text{Hz}}$; the current noise is about 2 pA/$\sqrt{\text{Hz}}$; and the unit-gain bandwidth is about 110 MHz. The gain of the amplifier is about 40 dB. A CG402R2 (NF Techno Commerce Co., Ltd., Yokohama, Japan) resister tunable oscillator was used to generate a sinusoidal signal, which was sent to the excitation coil, the compensation coil, and the reference port of the lock-in amplifier. The lock-in amplifier was composed of the analog multiplier of the AD633 (Analog Devices, Inc., Cambridge, MA, USA). Two AD633s were used; one was used to obtain the X signal and another was used to obtain the Y signal of the eddy current testing. After the output of the multipliers, low-pass filters with a bandwidth of about 100 Hz were used. An AI-1608GY-USB (Contec Co., Ltd., Osaka, Japan) AD converter was used to convert the analog signal to a digital signal. The resolution of the AD converter is 16 bit and it has eight input analog channels and a sample rate of up to 250 kHz. A USB cable was used to connect the AD converter with a computer. The power of the detection circuit and the AD converter was also supplied through the USB cable.

Figure 3 shows the setup of the experiments. The excitation coil, the detection coil, the amplifier, the lock-in amplifier, the signal generator, the phase shifter, and the AD converter were all put in a plastic probe box with a size of 85 mm × 170 mm × 60 mm. The excitation coil and the detection coil were attached on the bottom of the box. Only one USB cable was used to connect the probe to a computer for the data transfer and to supply power to the system. The electric power required by the circuit and the AD converter was less than 1 W (about 200 mA at 5 V). We developed a Labview program for data acquisition, data processing, data displaying, and data saving. The steel rebar was covered by concrete plates. The signal was obtained by moving the hand-held probe over the surface of the concrete plate.

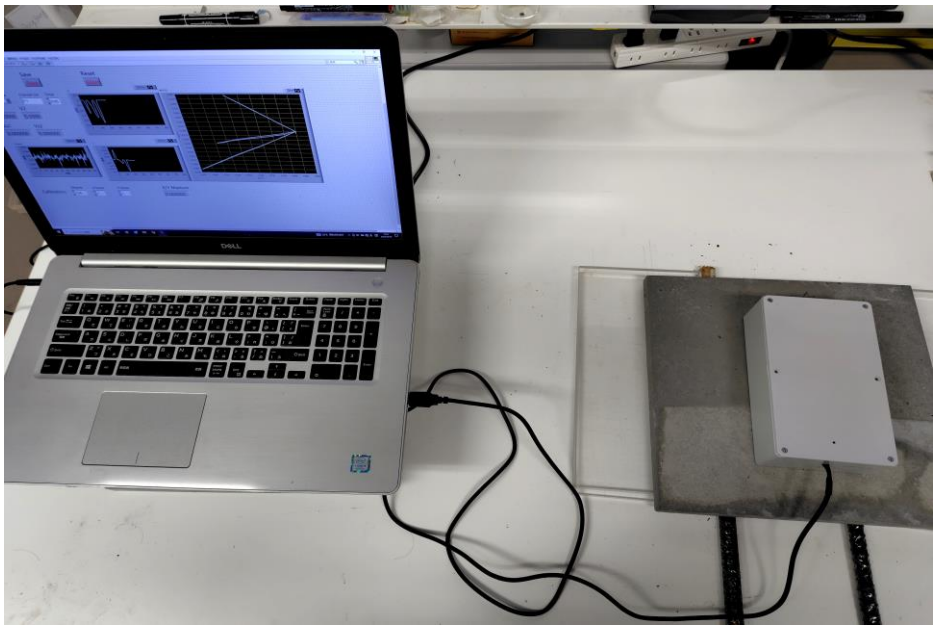


Figure 3. Setup of the experiments.

3. Results

For the eddy current testing nondestructive evaluation method, choosing the proper excitation frequency and the design of the probe is very important for defect detection, so

we examined the influences of the excitation frequencies, the coil types, and the coil sizes on the experimental results.

3.1. Influences of Different Excitation Frequencies

The influences of varying excitation frequencies on the experimental results were first examined. The excitation coil was a 50-turn toroidal type with a diameter of 5 cm. It was wound with 0.3 mm diameter copper wire. The detection coil was also a 50-turn toroidal type with a diameter of 1 cm. A 20-turn compensation coil with a diameter of 1 cm was put over the detection coil to compensate for the background signal produced by the excitation coil. The detection coil and the compensation coil were wound with 0.1 mm diameter copper wire. The current amplitude flow in the excitation coil was about 20 mA. The current flow in the compensation coil was adjusted by a potentiometer. Figure 4 shows the coils and the circuit in the probe.

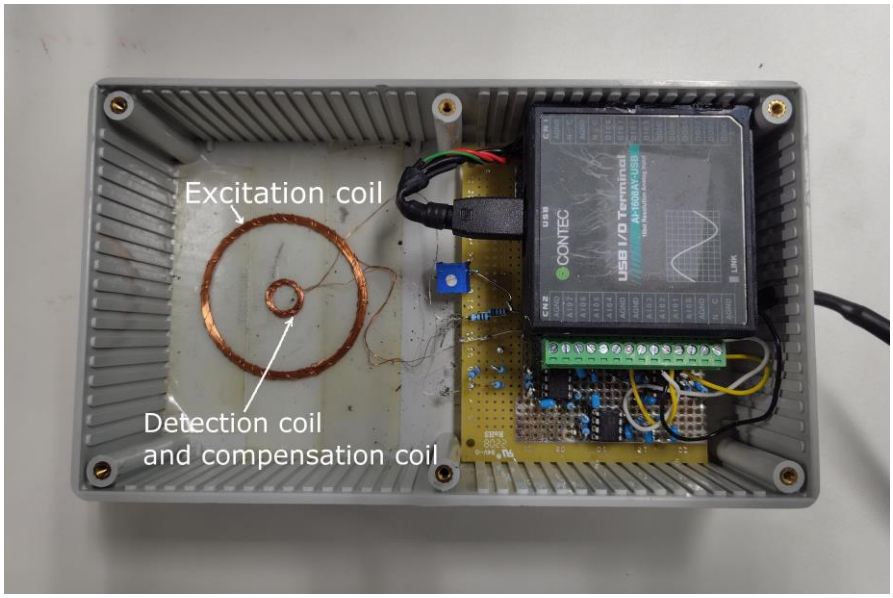


Figure 4. Excitation coil, detection coil, compensation coil, and the circuit in the probe.

Figure 5a shows the detected background signal without the compensation coil. The peak-to-peak amplitude was about 3.5 V when the excitation frequency was about 80 kHz. Figure 5b shows the detected signal with the compensation coil. The peak-to-peak amplitude was about 0.8 V. Because of the differences in the inductances of the excitation coil and the compensation coil, the current flow in the excitation and the compensation coil has some phase differences. Therefore, the background signal cannot be compensated completely. With a phase shifter, the compensation can be improved, but the complexity of the circuit will be increased.

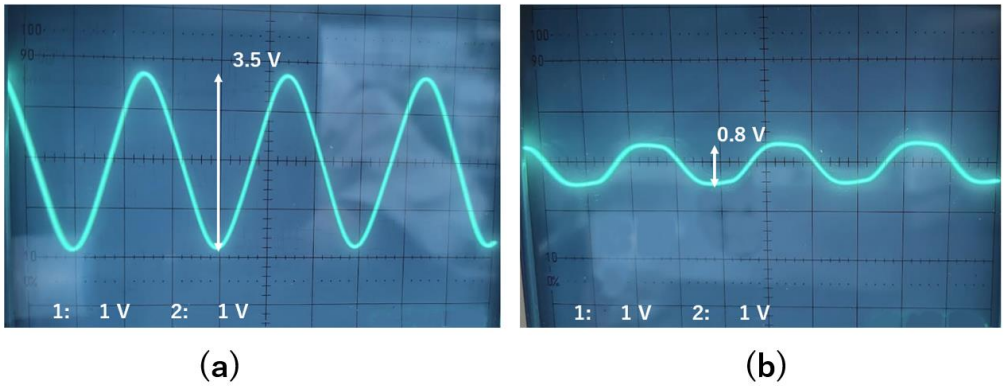


Figure 5. (**a**) Detected background signal without the compensation coil. (**b**) Detected signal with the compensation coil.

The depth of the steel rebar, which is the sum of the thickness of the concrete plate and the bottom thickness of the probe box, was about 25 mm. The excitation frequencies of 10 kHz, 40 kHz, 80 kHz, and 150 kHz were examined. Figure 6 shows the signals of the steel rebars with and without corrosion for different frequencies.

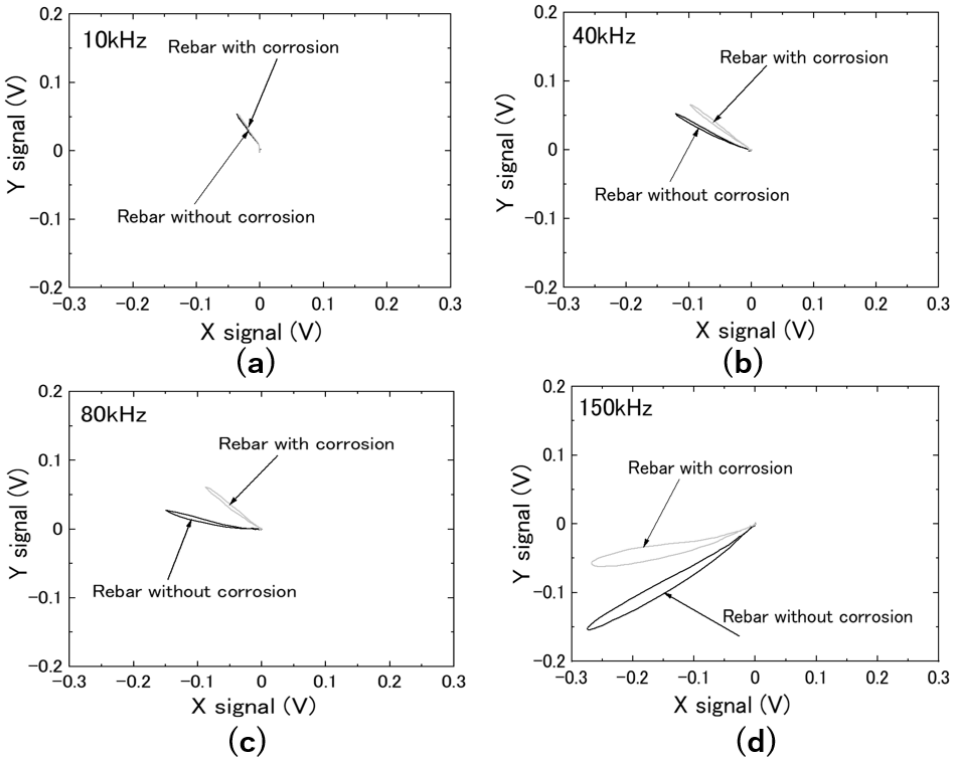


Figure 6. Signals of the steel rebars with and without corrosion for different frequencies. (**a**) 10 kHz. (**b**) 40 kHz. (**c**) 80 kHz. (**d**) 150 kHz.

Because the sensitivity of the detection coil increased with the frequency, the signal-to-noise ratio also increased with the excitation frequency. The phase difference of the signals for the steel rebars with and without corrosion also changed with the excitation frequencies. Figure 7 shows the results.

For the excitation frequencies of 10 kHz, 40 kHz, 80 kHz, and 150 kHz, the phase differences were 1.4°, 10.5°, 22.1°, and 18.9°, respectively. The phase difference was small at lower frequencies, such as 10 kHz. It was difficult to detect the corrosion of the steel rebar. With the increase in the excitation frequency, the phase difference also increased.

Among the four frequencies, the biggest phase difference of 22.1° was obtained at 80 kHz. At 150 kHz, a similar phase difference of 18.9° was obtained. However, the stability of the system became worse when the excitation frequency was 150 kHz. Therefore, we used 80 kHz in the following experiments.

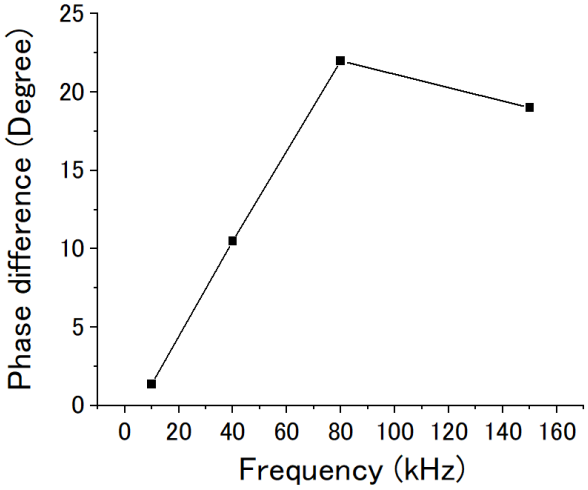


Figure 7. Phase differences of the signals for the steel rebar with and without corrosion when the excitation frequency was 10 kHz, 40 kHz, 80 kHz, and 150 kHz.

3.2. Toroidal Excitation Coils and Detection Coils

The toroidal coil is commonly used, and we examined the effect of different sizes of excitation coils on the experimental results. The excitation coils were 50-turn toroidal coils with diameters of 3 cm, 5 cm, 7 cm, and 9 cm, respectively. The detection coil and the compensation coil were the same as those used in 3.1. Figure 8 shows the excitation, detection, and compensation coils.

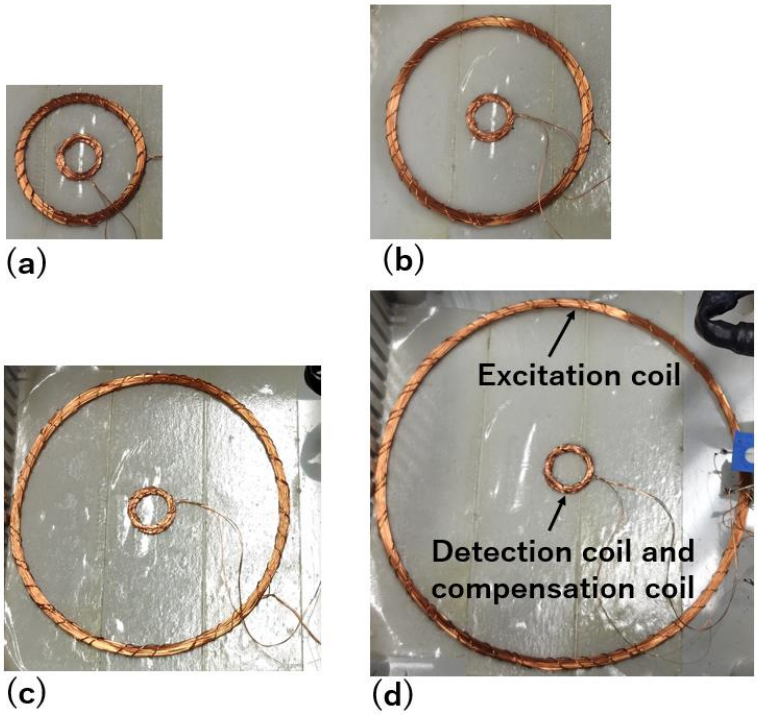


Figure 8. Excitation coil, detection coil, and compensation coil. (**a**) Excitation coil with a diameter of 3 cm. (**b**) Excitation coil with a diameter of 5 cm. (**c**) Excitation coil with a diameter of 7 cm. (**d**) Excitation coil with a diameter of 9 cm.

The current amplitude flow in the excitation coil was about 20 mA with an excitation frequency of 80 kHz. For each excitation coil, we measured the signals of the steel rebars with varying depths. Figures 9 and 10 show the signals for the excitation coils with different sizes when the depth was 25 mm and 45, respectively. The phase differences produced by the steel rebars with and without corrosion were similar for different sizes of excitation coils.

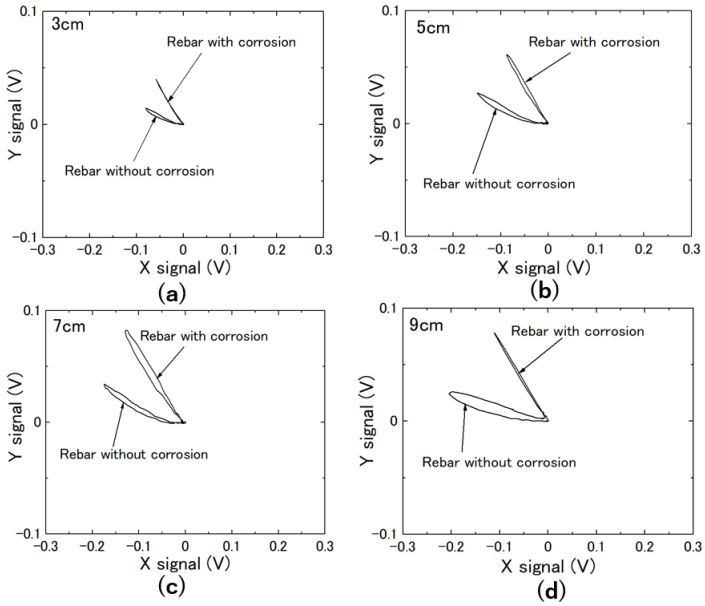


Figure 9. (**a**). Signals for the excitation coil with the diameter of 3 cm. (**b**). Signals for the excitation coil with the diameter of 5 cm. (**c**). Signals for the excitation coil with the diameter of 7 cm. (**d**). Signals for the excitation coil with the diameter of 9 cm. The depth of the steel rebar was 25 mm.

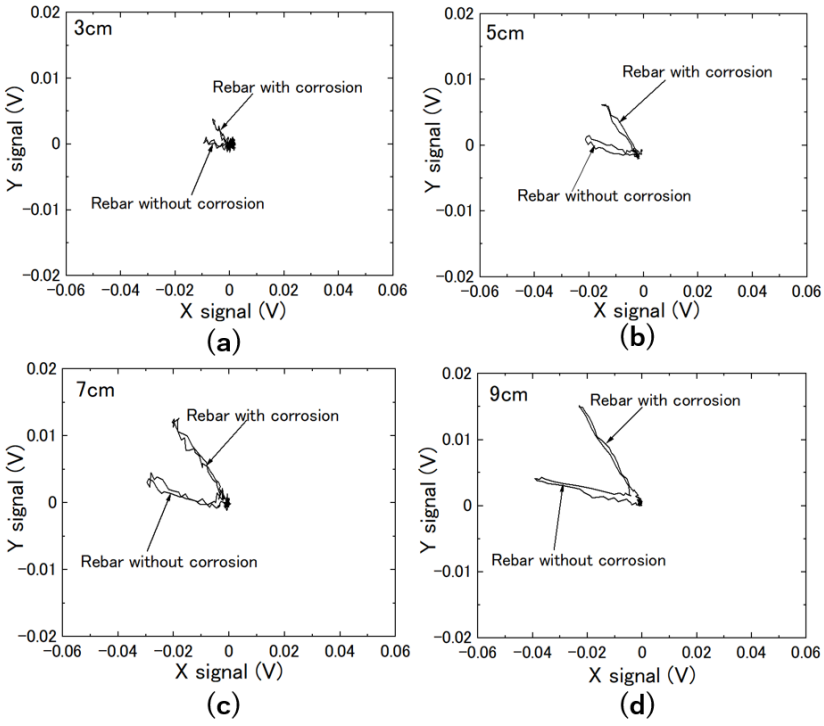


Figure 10. (**a**). Signals for the excitation coil with the diameter of 3 cm. (**b**). Signals for the excitation coil with the diameter of 5 cm. (**c**). Signals for the excitation coil with the diameter of 7 cm. (**d**). Signals for the excitation coil with the diameter of 9 cm. The depth of the steel rebar was 45 mm.

Figure 11 shows that the signal-to-noise ratios changed with the depths of the steel rebars for the excitation coils with diameters of 3 cm, 5 cm, 7 cm, and 9 cm. The signal-to-noise ratios decreased rapidly with the depth of the steel rebar. The maximum detection depth was proportional to the diameter of the excitation coil if the excitation current flow in the excitation coil was the same.

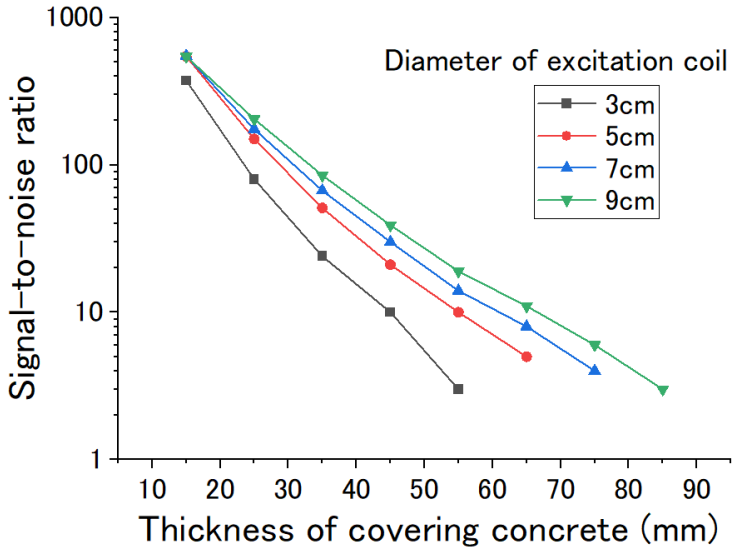


Figure 11. Signal-to-noise ratios changed with the depths of the steel rebars for the excitation coils with diameters of 3 cm, 5 cm, 7 cm, and 9 cm.

3.3. Differential Detection Coil with Helmholtz Excitation Coil

When a toroidal detection coil is used, the environmental noise might have an influence. A differential detection coil with a Helmholtz excitation coil was used to reduce the environmental noise's influence. Figure 12 shows it. The differential coil had two 50-turn coils with an inverse winding direction. The distance between the two coils was about 5 cm. The Helmholtz excitation coil had two 50-turn coils with the same winding direction. The distance between the two coils was 5 cm.

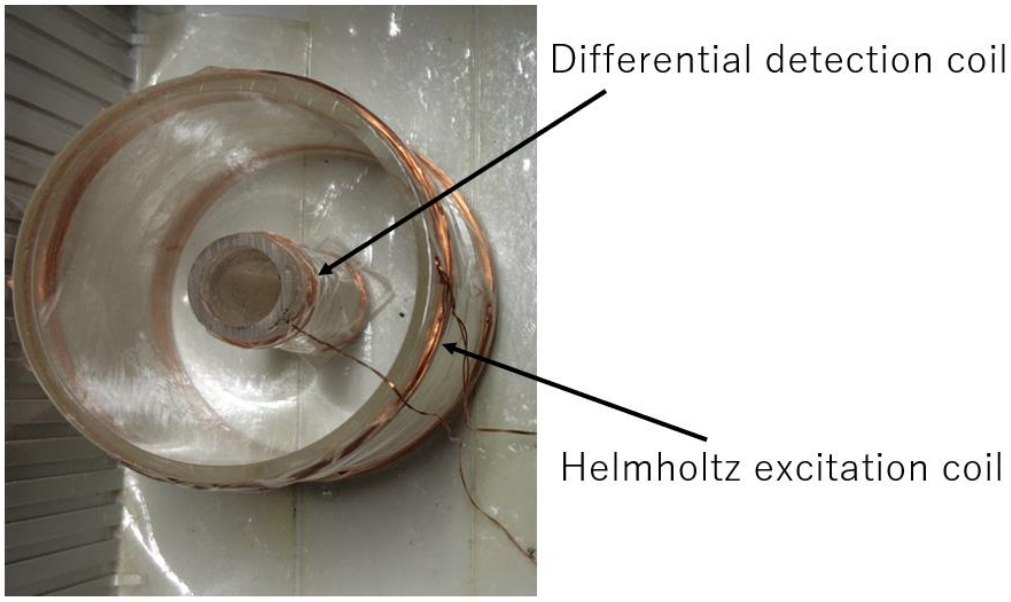


Figure 12. Differential detection coil with a Helmholtz excitation coil.

The excitation frequency was 80 kHz. The current amplitude flow in the excitation coil was about 20 mA. Figure 13 shows the detected signal after the amplifier. The peak-to-peak amplitude was about 10 mV. Compared with Figure 5, the compensation effect with the differential detection coil was about 80 times better than that with the toroidal detection coil. The ripple noise on the signal was caused by the PC switch power. With the lock-in amplifier, the noise had less influence on the results.

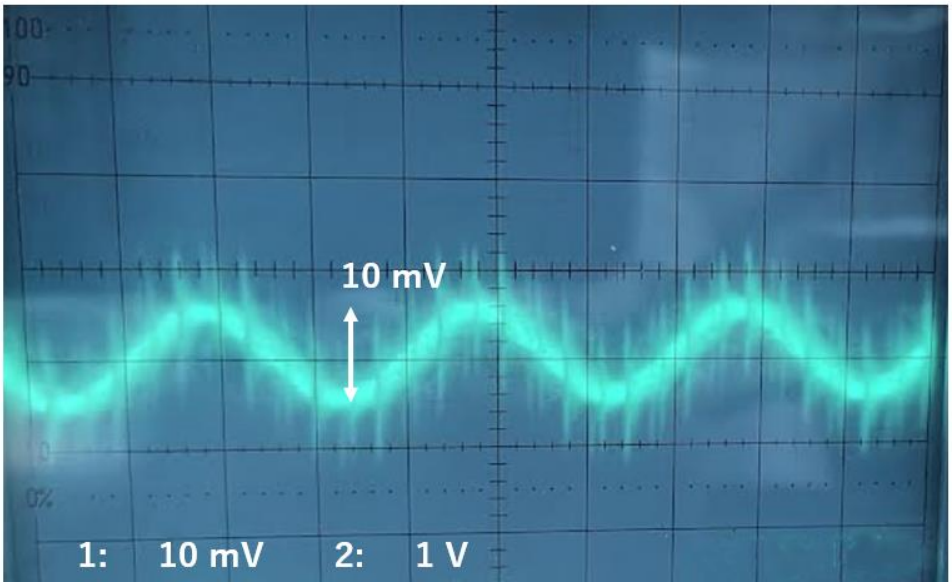


Figure 13. Background signal with the differential detection coil.

Figures 14 and 15 show the signals for the excitation coils with diameters of 3 cm, 5 cm, and 8 cm when the depths of the steel rebars were 25 mm and 45 mm, respectively. The phase differences produced by the steel rebars with and without corrosion were similar for different sizes of excitation coils.

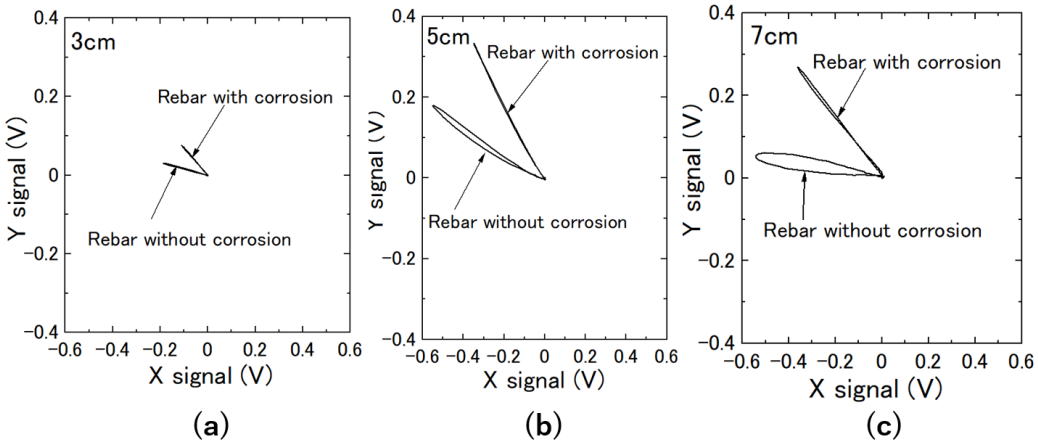


Figure 14. Signals for the differential detection coil with Helmholtz excitation coil when the depth of the steel rebar was 25 mm. (**a**). The diameter of the excitation was 3 cm. (**b**). The diameter of the excitation was 5 cm. (**c**). The diameter of the excitation was 7 cm.

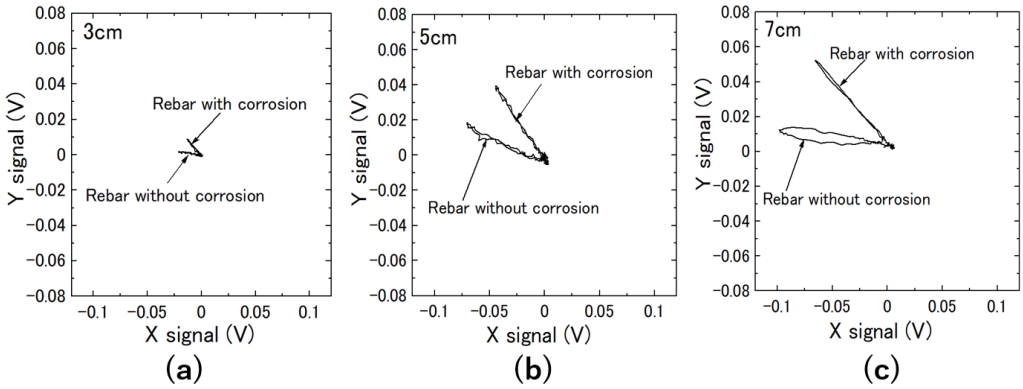


Figure 15. Signals for the differential detection coil with Helmholtz excitation coil when the depth of the steel rebar was 45 mm. (**a**). The diameter of the excitation was 3 cm. (**b**). The diameter of the excitation was 5 cm. (**c**). The diameter of the excitation was 7 cm.

Figure 16 shows that the signal-to-noise ratios changed with the depths of the steel rebars for the excitation coils with diameters of 3 cm, 5 cm, and 7 cm. The signal-to-noise ratios decreased rapidly with the depth of the steel rebar. Compared with the results achieved using toroidal coils, the signal-to-noise ratio was improved by over two times, and the maximum detection depth was improved by 1 cm for the excitation coil with the same diameter.

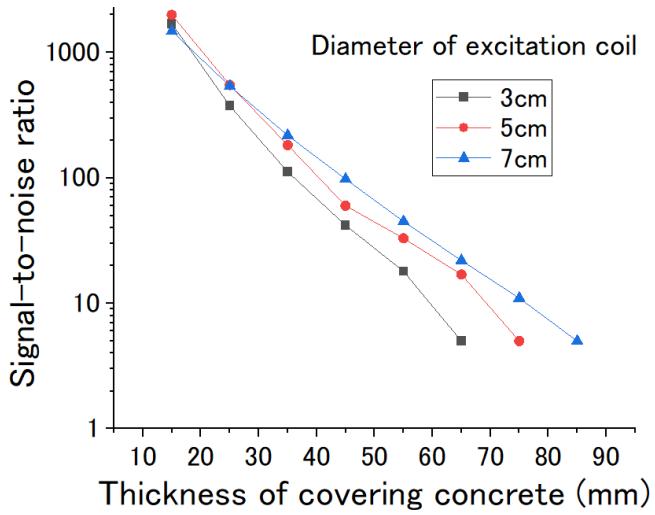


Figure 16. Signal-to-noise ratios changed with the depths of the steel rebars for the excitation coils with diameters of 3 cm, 5 cm, and 7 cm.

4. Discussion

Using the penetration depth of the eddy current, the measurement result shown in Figure 5 can be explained. The penetration depth of the eddy current can be calculated by

$$\delta \approx \frac{1}{\sqrt{\pi f \mu \sigma}} \tag{1}$$

where δ is the standard depth of penetration; f is the excitation frequency; μ is the magnetic permeability; and σ is the electrical conductivity. For the steel rebar, μ is about 2.51×10^{-4} H/m, σ is about 1.87×10^{6} S/m. The penetration depth is about 0.26 mm at 10 kHz, 0.13 mm at 40 kHz, 0.09 mm at 80 kHz, and 0.07 mm at 150 kHz. At lower frequencies, such as 10 kHz, the penetration depth of the eddy current is bigger, and the inside non-corrosion part of the steel rebar makes a big contribution to the signal, so the

signal difference is small for the steel rebar with and without corrosion (Figure 6a). At higher frequencies, such as 80 kHz, the penetration depth is small, and the surface condition of the steel rebar determines the signal, so the signal difference is big for the steel rebar with and without corrosion (Figure 6c).

Due to the low excitation frequency of 80 kHz used in our experiments, the variations in the temperature and the humidity have less influence on the signal. If the cement is mixed with conductive or magnetic substances, the signal will be affected, but this effect can be eliminated by multipoint measurements and data processing methods. As shown in Figure 9, the loop of the signal was caused by the surface shape of the steel rebar. It is possible to reduce the influence using the average value of the phase signals.

The adjacent steel rebar can also affect the signal. If the distance between the steel rebar is less than the sum of the covering depth and the diameter of the excitation coil, the effect of the adjacent rebar is not negligible. The depth and the distance between the steel rebars determine the selection of the diameter of the excitation coil.

To explain the difference between the toroidal coil and differential coil, we estimate the sensitivity of the measurement system. When the signal magnetic field B_S couples to the detection coil, the voltage amplitude generated on the coil is [28]

$$V_S = \frac{\pi^2 f N D^2 B_S}{2} \tag{2}$$

$$B_S = \frac{2V_S}{\pi^2 f N D^2} \tag{3}$$

where V_S is the voltage amplitude generated on the coil; f is the frequency; N is the turns of the detection coil; D is the diameter of the detection coil. In our experiments, f was 80 kHz, N was 50, and D was 5 cm. If the equivalent input voltage noise spectrum is Vn = 3 nV/$\sqrt{\text{Hz}}$, let $V_S = Vn$, and we can calculate the magnetic field resolution of the measurement system using Formula (3). Bn = 0.06 pT/$\sqrt{\text{Hz}}$. However, the environmental noise in the laboratory was at the level of 1 pT/$\sqrt{\text{Hz}}$, so, when a toroidal detection coil was used, the environmental noise was the main contributor to the noise of the output signal. The differential detection coil detects the gradient of the magnetic field. The environmental noise is a kind of far magnetic field, which is almost uniform and produces no output for the differential detection coil. The eddy current signal produces a local magnetic field. The local magnetic field has a bigger gradient and gives the output of the differential detection coil. Therefore, the influence of environmental noise can be reduced using the differential detection coil. The system with a differential detection coil has a better signal-to-noise ratio and a bigger detection depth.

Then, we used a PC and Labview program to carry out the data acquisition, data analysis, and result display. In the future, we will connect the probe to a Raspberry Pi signal board and develop a sensing network to monitor the corrosion of the steel rebar.

5. Conclusions

We developed a compact probe to detect the corrosion of steel rebars, and we also compared the results with a toroidal detection coil and differential detection coil. The signal-to-noise ratio and the detection depth were improved with the Helmholtz excitation and the differential detection coil.

Funding: This research was funded by Japan Cross-Ministerial Strategic Innovation Promotion Program (SIP): Construction of Smart Infrastructure Management System.

Institutional Review Board Statement: Not applicable.

Informed Consent Statement: Not applicable.

Data Availability Statement: Data are available upon request.

Acknowledgments: We thank T. Nishimura, H. Katsuhara, and K. Tsuchiya for the technical support and the discussion.

Conflicts of Interest: The authors declare no conflicts of interest.

References

1. Alhawat, M.; Zinkaah, O.H.; Araba, A. Study of corrosion products induced under different environmental conditions. *IOP Conf. Ser. Mater. Sci. Eng.* **2021**, *1090*, 012050. [CrossRef]
2. Robuschi, S.; Tengattini, A.; Dijkstra, J.; Fernandez, I.; Lundgren, K. A closer look at corrosion of steel reinforcement bars in concrete using 3D neutron and X-ray computed tomography. *Cem. Concr. Res.* **2021**, *144*, 106439. [CrossRef]
3. Steen, C.V.; Verstrynge, E. Degradation monitoring in reinforced concrete with 3D localization of rebar corrosion and related concrete cracking. *Appl. Sci.* **2021**, *11*, 6772. [CrossRef]
4. Soleymani, H.R.; Ismail, M.E. Comparing corrosion measurement methods to assess the corrosion activity of laboratory OPC and HPC concrete specimens. *Cem. Concr. Res.* **2004**, *34*, 2037–2044. [CrossRef]
5. Flis, J.; Sabol, S.; Pickering, H.W.; Sehgal, A.; Osseo-Asare, K.; Cady, P.D. Electrochemical measurements on concrete bridges for evaluation of reinforcement corrosion rates. *Corrosion* **1993**, *49*, 601–613. [CrossRef]
6. Morris, W.; Vico, A.; Vazquez, M.; de Sanchez, S.R. Corrosion of reinforcing steel evaluated by means of concrete resistivity measurements. *Corros. Sci.* **2002**, *44*, 81–99. [CrossRef]
7. Gowers, K.R.; Millard, S.G.; Gill, J.S.; Gill, R.P. Programmable linear polarisation meter for determination of corrosion rate of reinforcement in concrete structures. *Brit. Corr. J.* **1994**, *29*, 25–32. [CrossRef]
8. Liu, X.; Qin, L.; Huang, B. Huang Ultrasonic guided wave for monitoring corrosion of steel bar. *Conf. Ser. Earth Environ. Sci.* **2018**, *108*, 022071. [CrossRef]
9. Ghorbanpoor, A. Magnetic-based NDE of steel in prestressed and post-tensioned concrete bridges. In Proceedings of the Structural Materials Technology III, San Antonio, TX, USA, 31 March–3 April 1998; pp. 343–349.
10. Thomas, W.; Thomas, V. Detection of reinforcement breaks on large-scale fatigue tests with the magnetic flux leakage method. In Proceedings of the 8th fib PhD Symposium in Kgs, Lyngby, Denmark, 20–23 June 2010; pp. 587–592.
11. Perin, D.; Goktepe, M. Inspection of rebars in concrete blocks. *Int. J. Appl. Electromagn. Mech.* **2012**, *38*, 65–78. [CrossRef]
12. Gaydecki, P.A.; Burdekin, F.M. An inductive scanning system for two dimensional imaging of reinforcing components in concrete structures. *Meas. Sci. Technol.* **1994**, *5*, 1272–1280. [CrossRef]
13. Yu, Z.Z.; Gaydecki, P.A.; Silva, I.; Fernandes, B.T.; Burdekin, F.M. Magnetic field imaging of steel reinforcing bars in concrete using portable scanning systems. *Rev. Prog. Quant. Nondestruct. Eval.* **1999**, *18*, 2145–2152.
14. Gaydecki, P.; Silva, I.; Fernandes, B.T.; Yu, Z.Z. A portable inductive scanning system for imaging steel-reinforcing bars embedded within concrete. *Sens. Actuators A* **2000**, *84*, 25–32. [CrossRef]
15. Miller, G.; Gaydecki, P.; Quek, S.; Fernandes, B.; Zaid, M. A combined Q and heterodyne sensor incorporating real-time DSP for reinforcement imaging, corrosion detection and material characterization. *Sens. Actuators A Phys.* **2005**, *121*, 339–346. [CrossRef]
16. Ricken, W.; Mehlhorn, G.; Becker, W. Determining of the concrete cover thickness and the bar diameter in reinforced concrete with a method of eddy current testing. In Proceedings of the International Symposium Non-Destructive Testing in Civil Engineering (NDT-CE), Berlin, Germany, 26–28 September 1995; pp. 197–204.
17. Miller, G.; Gaydecki, P.; Quek, S.; Fernandes, B.T.; Zaid, M.A.M. Detection and imaging of surface corrosion on steel reinforcing bars using a phase-sensitive inductive sensor intended for use with concrete. *NDT&E Int.* **2003**, *36*, 19–26.
18. Bungey, J.H.; Millard, S.G. Radar inspection of structures. In Proceedings of the Institution of Civil Engineers—Structures and Buildings, London, UK, 15 July 1993; Volume 99, pp. 173–178.
19. Molyneaux, T.C.K.; Millard, S.G.; Bungey, J.H.; Zhou, J.Q. Radar assessment of structural concrete using neural networks. *NDT&E Int.* **1995**, *28*, 281–288.
20. Shaw, M.R.; Millard, S.G.; Molyneaux, T.C.K.; Taylor, M.J.; Bungey, J.H. Location of steel reinforcement in concrete using ground penetrating radar and neural networks. *NDT&E Int.* **2005**, *38*, 203–212.
21. Keo, S.A.; Brachelet, F.; Breaban, F.; Defer, D. Steel detection in reinforced concrete wall by microwave infrared thermography. *NDT&E Int.* **2014**, *62*, 172–177.
22. He, Y.; Tian, G.; Pan, M.; Chen, D. Eddy current pulsed phase thermography and feature extraction. *Appl. Phys. Lett.* **2013**, *103*, 084104.
23. Robuschi, S.; Tengattini, A. Corrosion of Steel in Concrete Seen through Neutron and X-Ray Tomography. *Neutron News* **2021**, *32*, 8-4. [CrossRef]
24. Dong, B.; Fang, G.; Liu, Y.; Dong, P.; Zhang, J.; Xing, F.; Hong, S. Monitoring reinforcement corrosion and corrosion-induced cracking by X-ray microcomputed tomography method. *Cem. Concr. Res.* **2017**, *100*, 311–321. [CrossRef]
25. He, D. Corrosion evaluation of steel rebar using electromagnetic induction method. *Stud. Appl. Electromagn. Mech.* **2020**, 141–146. [CrossRef]
26. He, D. Surface corrosion evaluation of steel cable for suspension bridge using electromagnetic method. *Surf. Sci. Tech.* **2023**, *1*, 16. [CrossRef]

27. Sordiashie, E. Electromagnetic Harvesting to Power Energy Management Sensors in the Built Environment. 2012. Available online: https://digitalcommons.unl.edu/cgi/viewcontent.cgi?article=1018&context=archengdiss (accessed on 30 October 2024).
28. Enpuku, K.; Morishige, T.; Mihaya, T.; Miyazai, T.; Matsuo, M.; Haku, S.; Yoshida, T. Magnetic Nanoparticle Imaging Using Cooled Pickup Coil and Harmonic Signal Detection. *Jpn. J. Appl. Phys.* **2013**, *52*, 087001. [CrossRef]

Disclaimer/Publisher's Note: The statements, opinions and data contained in all publications are solely those of the individual author(s) and contributor(s) and not of MDPI and/or the editor(s). MDPI and/or the editor(s) disclaim responsibility for any injury to people or property resulting from any ideas, methods, instructions or products referred to in the content.